Catalysis Today 427 (2024) 114439

Contents lists available at ScienceDirect

Catalysis Today

journal homepage: www.elsevier.com/locate/cattod

Application of zeolites for the production of biofuels and furans from hexose sugars in ethanol

B. Torres-Olea [a], A. Pérez-Merchán [a], P. Díaz-Maizkurrena [b], J.M. Requies [b], R. Moreno-Tost [a], J.A. Cecilia [a], C. García-Sancho [a,*], P. Maireles-Torres [a]

[a] Departamento de Química Inorganica, Cristalografía y Mineralogía, Facultad de Ciencias, Universidad de Malaga, Campus de Teatinos, 29071 Malaga, Spain
[b] Chemical and Environmental Engineering Department. Engineering Faculty of Bilbao, University of Basque Country (UPV/EHU), Plaza Ingeniero Torres Quevedo 1 e 48013, Bilbao, Spain

ARTICLE INFO

Keywords:
5-hydroxymethylfurfural
5-ethoxymethylfurfural
Glucose
Dehydration
Etherification
Zeolite

ABSTRACT

The use of zeolites as catalysts in the transformation of glucose and 5-hydroxymethylfurfural (HMF) into 5-ethoxymethylfurfural (EMF) was evaluated. The behaviour of the catalysts could be explained by their morphology, composition, acid properties and chemical coordination of the active sites. The progress of the reaction was followed by High Performance Liquid Chromatography (HPLC) and ^{13}C Nuclear Magnetic Resonance (NMR). Several intermediates were identified, and a reaction path is proposed. Different cosolvents were also employed in this study to enhance the selectivity towards different possible valuable compounds, and they were found to have a positive influence for the production of EMF and furfural.

1. Introduction

The upgrading of biomass-derived compounds has gained attention in the last decades for the replacement of non-renewable resources. An example is the production of furanic compounds from hexoses. In this sense, C6 sugars can undergo sequential dehydration to give rise to HMF, a precursor for potentially useful compounds, such as biofuels and monomers for polymer synthesis [1–4]. Biofuels with high energy density and miscibility with conventional fuels can be obtained using catalytic amounts of acids and alcohols in the presence of HMF. HMF is then etherified into 5-alkoxymethylfurans, like 5-methoxymethylfuran and EMF, depending on the alcohol employed [3,5–10]. In this process, other valuable chemicals are also produced, since levulinic acid or ethyl levulinate can be originated when HMF or EMF suffer rehydration. Alkyl levulinates have been studied for their biofuel applications, while levulinic acid can be used as a platform chemical, precursor of other high value-added chemicals and polymers [11–13].

Many catalysts have been investigated so far to carry out the synthesis of HMF and subsequent etherification to originate biofuels, including heteropolyacids [5,6,14], sulphonated polymers [7,15], meso-structured silicas [16,17], metal oxides, zeolites [18–21], ionic liquids [22] and inorganic salts [23,24]. However, HMF is too costly to be directly employed in the production of biofuels or other chemicals, and processes that convert widely available hexoses directly to upgraded products are being developed [3]. The reactivity of hexoses varies greatly depending on whether they occur in their ketose (fructose, tagatose, etc.) or aldose form (glucose, galactose, etc.). Ketoses can be easily converted into HMF through the use of Brønsted acid catalysts. Overall, many papers have reported the transformation of ketoses in HMF derivatives. Zong et al. utilised sulphonated mesoporous silica-carbon composites to dehydrate fructose and produce biofuels in ethanol, and obtained 63% yield of HMF ethers at 140 ºC after 6 h [17]. In contrast, when they tried to apply the same catalyst to the valorisation of glucose, only minor amounts of HMF derivatives were detected, being the etherification of glucose the preferent pathway. Similarly, Yang et al. employed an heteropolytungstate acid to obtain EMF from fructose in a one-step process [5]. A 65% EMF yield was observed in ethanol after 30 min at 130 ºC. Still, when using glucose as a feedstock, the only products found were ethylglucosides, not furans or derivatives. The dehydration of aldoses into valuable chemicals remains, currently, a challenge [3,5,8]. It is generally accepted that aldoses usually require to isomerize first before dehydrating into HMF. In the presence of alcohols and Brønsted acid sites, aldoses evolve by etherifying rather than dehydrating or isomerizing to form reactive ketoses. Instead, Lewis acid sites are needed to promote this process. This was observed in a previous work in which the use of alumina, as provider of Lewis acid sites, and a sulphonated

* Corresponding author.
E-mail address: cristinags@uma.es (C. García-Sancho).

https://doi.org/10.1016/j.cattod.2023.114439
Received 13 July 2023; Received in revised form 29 September 2023; Accepted 22 October 2023
Available online 24 October 2023

polymer, with Brønsted acid sites, were required to enable the production of HMF and HMF derivatives from glucose. An EMF yield of 26% was achieved after 3 h at 140 ºC using both materials.

In addition, even in the presence of Lewis acid catalysts, the observed HMF yields are usually low when working with aldoses. This has led to exploiting the effect of cosolvents to influence the preferential isomeric form in aldoses and ketoses, or the utilization of multiple catalysts into the reaction media [5,19,25]. Indeed, Chen et al. observed that the EMF yield increased when corn stover was treated with USY zeolite in an ethanol:THF (2:3, v/v) solution for 2.5 h and 180 ºC, since the EMF yield was increased from 9% when using ethanol as the sole solvent up to 15% in the solvent mixture [19], while Zheng et al. used USY to transform glucose into EMF in a one pot process achieving a final EMF yield of 40% [21]. On the other hand, Xin et al. combined $AlCl_3$ with PTSA-POM to catalyse the transformation of glucose and attained a 60% HMF yield in a water:GVL system, but cosolvents failed to show a positive effect on EMF production when using an ethanol:water:cosolvent mixture in a single step from glucose [25]. Despite all the advances and research on the production of HMF, its derivatives and other interesting secondary products, the production of EMF utilizing solid acid catalysts still has ample room for improvement.

Hereby, we report the behaviour of commercial zeolites with different Si:Al molar ratio in the transformation of biomass-derived compounds to biofuels and other platform molecules. In this work, the morphology of the zeolites employed as catalysts has been identified as the single most important factor in the activity of the material towards the etherification of HMF into EMF, more than the acidity or composition of the zeolites. The beta zeolite has been found to be the most adequate to carry out the transformation from glucose. The reaction was followed by ^{13}C NMR, which provided vital information to propose a reaction path. Furthermore, the effects of several cosolvent have been studied, and methyl isobutyl ketone has proved to be the most beneficial cosolvent for the production on EMF studied in this research.

2. Materials and methods

2.1. Reagents

The following reagents were employed in this work: ethanol (96%, VWR Chemicals), γ-valerolactone (GVL) (>99%, Sigma-Aldrich), tetrahydrofuran (THF) (>99.9%, Aldrich), methyl isobutyl ketone (MIBK) (>99%, VWR Chemicals), glucose (>99%, Sigma-Aldrich), fructose (>99%, Sigma-Aldrich), HMF (>99.9%, Sigma-Aldrich), EMF (97%, Sigma-Aldrich).

Several commercial zeolites, supplied by Zeolyst, were employed in this study. They were characterised and named after their structure, followed by their Si/Al molar ratio for easier interpretation of the data. Commercial names are given between parentheses. ZSM5–9 (CBV2314), ZSM5–15 (CBV3024E), ZSM5–23 (CBV5524G), Beta–10 (CP814E), Beta–16 (CP814C), Beta–96 (CP814C–300), FER–10 (CP914C). Zeolites in ammonium form were submitted to calcination at 450 ºC for 6 h to obtain the corresponding hydrogen form.

2.2. Reaction procedure

All reactions were carried out in glass pressure reactors (thread bushing, Ace, 15 ml), generally employing 5 ml of ethanol as solvent, unless otherwise specified, 0.1 g HMF (or 0.15 g hexose), 0.05 g of catalyst, under an autogenous pressure generated by heating at different temperatures (140, 160 and 180 ºC). All reactors were purged with N_2 previous to the reaction to eliminate oxygen from the reaction media and avoid unwanted oxidation processes. After that, they were introduced in an aluminium block at a controlled temperature with magnetic stirring (450 rpm) to provide homogeneous heating. Once the reaction was over, the reactor was submerged in water at room temperature to quench the process. As soon as it was cooled, the reactors' contents were diluted with 2.15 ml of water and prepared to be analysed by high-performance liquid chromatography (HPLC).

2.3. Product analysis

Analyses were carried out using a JASCO HPLC. The mobile phase consisted of 0.4 ml·min^{-1} pure microfiltered water pumped by a quaternary gradient pump (PU-2089). Products were separated in a Phenomenex REZEX Ca^{2+} Monosaccharide column (300 mm × 7.8 mm) heated at in a column oven (CO-2065) at 70 ºC. Separated products were quantified using both a refractive index detector (RI-2031-PLUS) and a multiwavelength detector (MD-2015) that recorded the absorption at 278 nm. In all cases, except when MIBK was used as cosolvent, once the reactor had cooled down, the reactor's contents were diluted with 2.15 ml of water, this assures the solubility of all reagents at room temperature, and was prepared to be analysed by HPLC.

When MIBK was used as cosolvent, the sample was analysed by using a Phenomenex Luna C18 reversed-phase column (250 mm × 4.6 mm and 5 μm) for HPLC and a flow of 0.4 ml·min^{-1} of methanol, while the presence or absence of furfural was checked by a Gas Chromatograph (Shimadzu GC-14A) with a flame ionization detector and a CP-Wax 52 CB capillary column. The heating ramp was set to 40 ºC for 5 min, before heating at 10 ºC per minute up to 280 ºC. Then, it was followed by a plateau at 280 ºC for 1 min. The amount of sample introduced was 1 μl. O-xylene was used as the internal standard. Polar components were extracted from the solution using water that was analysed by reverse phase chromatography using Phenomenex REZEX Ca^{2+} Monosaccharide column (8%) (300 mm × 7.8 mm, 5 μm).

Conversion, selectivity and yield were calculated as follows:

$$\text{Conversion}_Y = \left(\left(\text{mol}_{\text{initialY}} - \text{mol}_{\text{finalY}}\right)/\text{mol}_{\text{initialY}}\right)\cdot 100 \quad (1)$$

$$\text{Selectivity}_X = \left(\text{mol}_{\text{finalX}}/\left(\text{mol}_{\text{initialY}} - \text{mol}_{\text{finalY}}\right)\right)\cdot 100 \quad (2)$$

$$\text{Yield}_X = \left(\text{Selectivity}_X\cdot\text{Conversion}_Y\right)/100 \quad (3)$$

$$\textit{Carbon Balance} = \left(mol_{finalX1} + mol_{finalx2} + mol_{finalx3}\ldots\right)/mol_{initialY} \quad (4)$$

Where Y is the initial feedstock (HMF or Glucose as indicated in each experiment), while X refers to the products and intermediates resultant of the feedstock transformation. x_1, x_2, x_3, refer to the different compounds quantified after the reaction.

2.4. Catalyst characterization

N_2 adsorption-desorption isotherms were obtained using an automatic ASAP 2420 from Micrometrics at − 196 ºC. Prior the analysis, the samples were evacuated at 200 ºC and 10^{-4} bar. The specific surface area was calculated using the Langmuir equation [26], Density Functional Theory [27] and MP method [28] were employed to determine pore size distributions. N_2 cross-section was considered 16.2 Å^2.

The acidity of the zeolites was measured by means of NH_3-TPD. The analysis was carried out in a AutoChem II Instrument (Micrometrics, USA), equipped with a TCD detector. The samples were heated up to 200 ºC for 6 h, then, they were cooled to 100 ºC and, at this point, NH_3 (10% v/v of NH_3 diluted in He) was fed to the sample for 30 min. The physisorbed NH_3 was removed with He for 30 min. Chemisorbed NH_3 was evolved heating the sample up to 800 ºC at a rate of 10 ºC·min^{-1} and detected by a TCD.

The concentrations of Brønsted and Lewis acid sites (BAS and LAS, respectively) were determined by FTIR spectroscopy (1400–1700 cm^{-1}) after pyridine adsorption at 150 °C onto the self-supported sample, in vacuum, by using a Specac catalytic chamber connected on-line with a Nicolet 6700 FTIR spectrometer. The results were determined from the ratio between the intensity of pyridine absorption bands at 1545 and 1450 cm^{-1} and taking into account the molar extinction coefficients

proposed by Emeis for both absorption bands ($\varepsilon_B = 1.67$ cm μmol^{-1} and $\varepsilon_L = 2.22$ cm μmol^{-1}) [29].

X-ray Photoelectron Spectra (XPS) were recorded in a Physical Electronics PHI 5700, with a multichannel detector and non-monochromatic Mg K_α radiation (300 W, 15 kV, 1253.6 eV). Spectra were taken in pass-energy mode at 29.35 eV and a diameter area of 720 μm and calibrated using adventitious carbon at 284.8 eV. PHI ACCESS ESCA-V 6.0 F software package was employed to record and treat XPS data. Peaks were fitted using a Gaussian-Lorentzian curve, and a Shirley type background was subtracted from the signals.

The chemical composition of the catalysts was determined by inductively coupled plasma-optical emission spectrometry (ICP-OES) by an Optima 7300DV (Perkin Elmer) with automatic sampler, pneumatic concentric nebulizer, spray cyclonic chamber and quartz torch. Two solid detectors were used with a wavelength range between 163 and 782 nm.

Powder X-ray diffraction patterns were obtained on a Philips EMPYREAN automated diffractometer using Cu $K_{\alpha1,2}$ (1.5406 Å) and a PIXcel detector. Divergence and anti-divergence slits were fixed at 1/4º and 1/2º Soller slits, respectively, for incident and refracted rays were employed at 0.04 rads. Measures were taken from 5 to 80º (2θ) for approximately 30 min with a step size of 0.0167º. The X-ray tube voltage employed was 45 kV and current of 40 mA. The sample was rotated continuously to increase particle statistics.

Magic-angle spinning-nuclear magnetic resonance (MAS NMR) spectra of ^{27}Al were recorded with an AVANCE III HD 600 (Bruker AXS, Rheinstetten, Germany) using Hpdec technique. Samples were rotated with a speed of 20 kHz in 2.5 mm triple resonance DVT probes. 5000 scans were carried out for each sample with 1 s delay. Chemical shifts were referenced to $Al(NO_3)_3$. For the analysis, a magnetic field of 14.1 T corresponding to a ^{27}Al resonance frequency of 156.37 MHz was used.

Thermogravimetric analysis was recorded by a TA instruments (SDT-Q600 analyzer), using open platinum crucibles under air flow in the range of 30–600 °C and a heating rate of 10 °C·min^{-1}.

3. Result and discussion

The crystalline structures of zeolites were confirmed from their powder X-ray diffraction patterns (Fig. S1). The wide peaks are indicative of a slightly distorted structure, but, in all cases, the characteristic diffraction signals of the corresponding zeolitic structure were observed.

The zeolites show low mesoporosity, as can be inferred from the thin hysteresis loop in the N_2 adsorption-desorption isotherms at − 196 ºC (Fig. S2a) [30]. All zeolites exhibit very high specific surface areas, ranging between 420 and 740 m^2·g^{-1} (Table 1). However, the Langmuir surface area and t-plot micropore surface area indicate that most of the pores in these materials are of very small dimensions and may not be accessible to very large molecules. Nevertheless, pores with a size of at least 6 Å are needed for the HMF molecule to enter the cavity and take advantage of any possible shape selectivity or confinement, size that increases to at least 8.5 Å for hexoses [31]. According to the morphologic analysis, Beta–10 presented mesopores with a wide range of pore widths, from 4 to more than 25 nm, with a maximum at 8.75 nm, while, for the other zeolites, only pores with a width less than 4 nm could be detected, whose width cannot be determined through this method due to limitations of the technique [27]. In the DFT pore distribution (Fig. S2b), it is notable that most zeolites studied were found to lack mesopores, except zeolite Beta–10, which has a high range of pores wider than 5 nm. Also, employing MP method (Figs. S2c), 3 groups of pores are detected. In the first place, pores of more than 6 Å were seen in the beta zeolites: Beta–96 and Beta–16. Thus, wide surface area is available to molecules so that diffusion problems would not be the limiting factor in the process [32].

Table 1
Textural properties and chemical composition of the zeolites.

Zeolite	Given name	Langmuir surface area (m^2·g^{-1})	t-Plot micropore area (m^2·g^{-1})	Si/Al molar ratio	
				(XPS)	(ICP-OES)
CP914C	FER–10	432.0	413.3	11.4	10
CBV5524G	ZSM5–23	537.6	491.4	103.1	23
CBV3024	ZSM5–15	422.0	413.3	20.3	15
CBV2314	ZSM5–9	493.6	463.2	10.9	9
CP811C–300	Beta–95	666.5	588.8	292.9	95
CP814C	Beta–16	734.2	646.0	25.0	16
CP814E	Beta–10	726.8	530.9	14.1	10

Acid properties were evaluated from NH_3-TPD plots, where two distinct signals could be found in each zeolite. A first signal centered between 160 and 350 ºC would correspond to the desorption of NH_3 molecules adsorbed on medium strength acid sites, while the smaller band between 350 and 400 ºC is associated to molecules on strong acid sites. The concentration of both types of acid sites is presented in Fig. 1 and quantified in Table 2. For isostructural zeolites, the amount of both types of acid sites increases with the aluminum loading, as seen in the ZSM5 and Beta series. However, comparing the different types of zeolites, concentration and strength of acid sites can vary significantly, even for similar aluminum contents. Thus, FER–10 and ZSM5–9 zeolites possess a concentration of medium strength acid sites much higher than Beta–10, with very similar aluminum loading. The amount of acid sites increases with lowering the Si/Al molar ratio.

Hpdec ^{27}Al MAS NMR was also employed to characterize the zeolites. Signals were found at 0 and up to 60 ppm, that belong to hexacoordinated and tetrahedral sites, and thar provide with Lewis and Bronsted acid sites, respectively, (Fig. S3, Table 3) [33]. It is noteworthy that, increasing the aluminum content of the material within each structure type, ZSM5 and Beta, increased the percentage of aluminum in extra-framework octahedral positions.

Surface composition of the zeolites was determined by means of XPS. Except in the case of ZSM5–9, the rest of the materials possessed a superficial aluminium content smaller than expected according to the supplier's information. (Table 4, Fig. S4). The core level spectra corresponding to O 1 s revealed a binding energy (BE) that varied between 532.7 and 533.2, in accordance with what has been reported in literature. In the case of Si 2p, BE values were close to 103.4 eV for Beta zeolites, except for Beta–96, whose value was 103.9 eV, similar values to those found for SiO_2 [37,38]. Al 2p BE shifted, within each zeolite type, with increasing concentration of surface Al species, from 74.2 to 75.0 eV, as shown in Table 5, values in accordance with other BEs reported in the literature [34–37]. XPS analysis detected quantities of aluminium that can be as 50% smaller than those reported by ICP analysis, which could be explained by the existence of an aluminium rich core and silicon rich surface. ^{27}Al RMN analysis, which detected

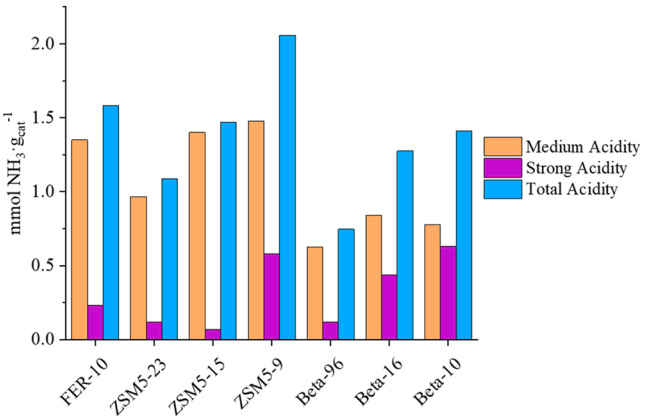

Fig. 1. NH_3-TPD histograms of zeolites: medium (NH_3 desorbed below 350 ºC) and strong (NH_3 desorbed between 350 and 400 ºC) acid sites.

Table 2
Acidity of the zeolites measured by NH_3-TPD and pyridine adsorption coupled to FTIR spectroscopy.

Catalyst	Concentration of acid sites mmol·g^{-1}		Brønsted/Lewis acid sites ratio
	Medium	Strong	
FER–10	1.35	0.23	27.9
ZSM5–23	0.97	0.12	3.9
ZSM5–15	1.40	0.07	7.2
ZSM5–9	1.48	0.58	28.6
Beta–95	0.63	0.12	0.16
Beta–16	0.84	0.44	0.6
Beta–10	0.78	0.63	0.6

Table 3
^{27}Al NMR signals detected for each zeolite, in percentage.

Zeolite	< 10 ppm	39–44 ppm	50–60 ppm	> 60 ppm
FER–10	0.5	16.4	83.1	0
ZSM5–23	6.0	0	94	0
ZSM5–15	13.2	0	86.8	0
ZSM5–9	22.3	16.0	35.8	25.9
Beta–95	0	0	100	0
Beta–16	14.2	10.4	48.8	26.6
Beta–10	24.6	0	75.4	0

Table 4
Surface composition of the zeolites given by XPS analysis.

Zeolite	%Al	%Si	%O	O/ (Al+Si)	Al/ (O+Si)
FER–10	2.6	29.6	58.3	2.0	0.02
ZSM5–23	0.3	32.1	67.6	1.92	0.01
ZSM5–15	1.8	35.8	68.5	1.81	0.03
ZSM5–9	2.9	31.2	65.9	1.90	0.03
Beta–96	0.1	32.5	67.3	1.88	0.002
Beta–16	1.1	28.1	58.2	1.94	0.013
Beta–10	2.3	33.0	64.6	1.83	0.02

Table 5
Binding energies for the main elements obtained from XPS analysis.

Zeolite	C 1 s			O 1 s	Si 2p	Al 2p
FER–10	289.0	287.4	284.8	532.2	102.9	74.7
ZSM5–23	289.5	287.4	284.8	532.7	103.3	74.5
ZSM5–15	289.3	286.8	284.8	532.4	103.1	74.6
ZSM5–9	289.6	287.2	284.8	532.3	103.6	74.7
Beta–95	289.7	287.4	284.8	533.2	103.9	74.2
Beta–16	289.9	287.2	284.8	532.7	103.4	74.4
Beta–10	289.9	287.3	284.8	532.6	103.3	74.8

extra-framework hexacoordinated aluminium species (signal close to 0 ppm). At the same time, the surface seems to be deficient in oxygen, being less than 2:1, the ratio expected for SiO_2, but this could also be explained by the existence of surface Al_2O_3. As previously mentioned, uncoordinated metals are susceptible to act as Lewis acid sites, useful in aldose isomerization to ketoses.

3.1. HMF etherification: screening

The zeolites with different frameworks and Si:Al molar ratios were screened for the production of EMF by etherification of HMF with ethanol, at 140 °C and 160 °C for 3 h (Fig. 2a). When silicon is substituted with aluminium in a zeolite framework, the structure gains a net negative charge, thus requiring cationic species to achieve the neutrality. In the present work, as the zeolites are in their protonic form, an increase in the aluminum content will increase the concentration of cationic H^+ species and, consequently, the amount of Brønsted acid sites. HMF etherification requires the participation of these Brønsted acid sites. This correlates well with the fact that, within the same zeolite type, the formation of EMF increases linearly with the aluminum content present in the zeolites (Figs. 3a, 3b). Beta zeolites with higher aluminum content produced higher EMF yield and selectivity values, with Beta–10 zeolite achieving a 95% HMF conversion with 77% EMF yield. However, ZSM5 and FER–10 zeolites performed poorly even with an elevated number of acid sites, as determined by NH_3-TPD, medium strength in the case of FER–10, and total acidity in the case of ZSM5–9. In fact, FER–10 zeolite was almost inactive as catalyst in this process. It is noteworthy that the amount of acid sites, of strong acid sites, in Beta zeolites and their corresponding yield of EMF were closely correlated. (Fig. 3c). The linear relationship between the two parameters suggests that these strong acid sites are directly involved in the etherification process.

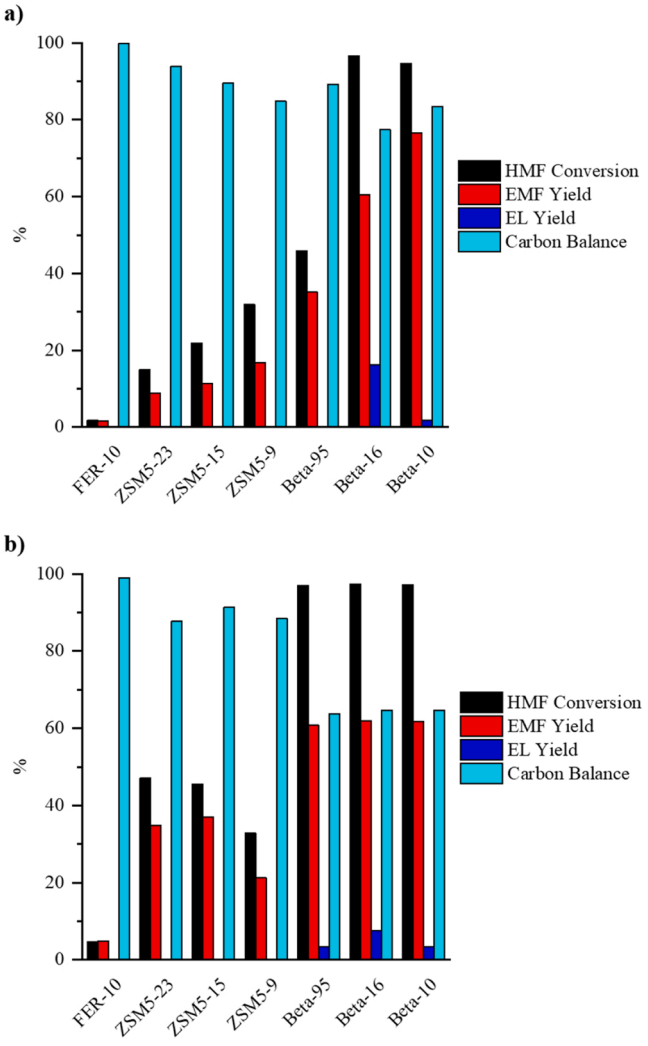

Fig. 2. HMF etherification with ethanol at: a) 140 °C and b) 160 °C (Experimental conditions: 0.1 g HMF, 0.05 g zeolite, 5 ml of ethanol, 3 h).

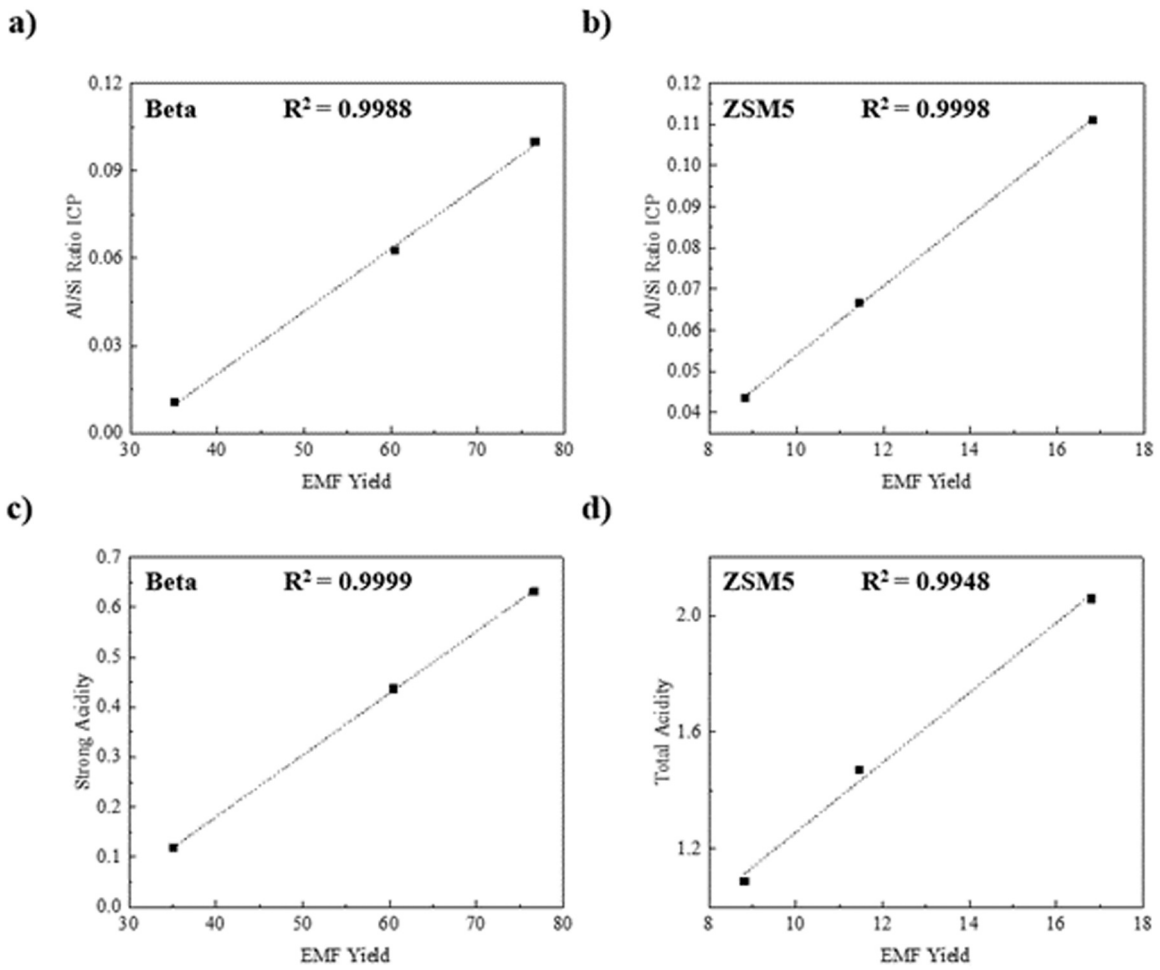

Fig. 3. Representation of EMF Yield a) against ICP Al/Si ratio for Beta zeolites, b) against ICP Al/Si ratio for ZSM5 zeolites, b) Strong acid sites found in Beta zeolites, c) Total acidity found in ZSM5 zeolites (0.05 g zeolite, 0.1 g HMF, 140 ºC, 3 h).

Similarly, close relationship was found between the total amount of acid sites present in ZSM5 and the EMF yield (Fig. 3d).

Thus, for the same type or zeolite, the catalytic activity in the etherification of HMF improves with the Al content, or number of acid sites, which could be easily explained by a higher Brønsted acidity provided by protons neutralizing charges. However, differences in catalytic performance are higher between different morphologies than within a single type and changing the aluminum content. In this sense, NH_3-TPD data would confirm that these differences are not due to the number of acid sites present in the materials, as in fact, the FER–10 and the ZSM5–9 have both higher concentration of acid sites than any beta zeolite. It has been previously reported that Beta zeolites in HMF etherification with ethanol showed a Turnover Frequencies (TOFs) one order of magnitude higher than the rest of the studied zeolites [39]. It was concluded that mass transfer effects or gradient effects were not the cause of the high selectivity of the beta zeolite towards the etherification of HMF to originate EMF. On the other hand, they stated that the HMF kinetic diameter is approximately 6.2 Å, close to the diameter of the bigger channels present in the BEA zeolites and suggested that it may play a role in stabilizing the HMF transition state. Indeed, ZSM5 zeolite structure resembles that of the Beta, but ZSM5 cavities and channels are significantly smaller. In our experiments at 140 ºC (Fig. 2a), results provided by ZSM5–9 and Beta–10 zeolites differ greatly despite their similar morphology and aluminium content, in such a way that Beta converted 63% more HMF (95% versus 32%) and attained a 60% extra EMF yield (76% versus 16%). Theoretically, diffusion within the internal channels and voids of the three types of zeolites (FER, ZSM5 and Beta) would not be possible, given their dimensions are smaller than the kinetic diameter of HMF. However, Beta zeolites showed wider cavities and channels, as inferred from their corresponding pore size distributions calculated by both,DFT and MP methods (Fig. S2) [40]. Thus, the reaction would proceed only on the external surface area and Beta zeolites (BEA structure) should be benefiting from form selectivity induced by the cavities of a size adequate to stabilize the transition state of HMF. Therefore, larger cavities seem to have a positive effect in HMF conversion and EMF selectivity under the studied experimental conditions, possibly allowing a suitable interaction between acid sites and HMF molecules. However, when the screening is carried out at 160 ºC, significant differences between beta zeolites were not detected, showing very high conversion values and EMF yields close to 61%; however, all of them show better catalytic performance than the rest of zeolites (Fig. 2b). Due to the use of a higher temperature, the kinetics of the process are now high enough, so that, in 3 h, the three materials achieved full conversion, independently from their concentration of acid sites. Small amounts of EL were also detected for the three Beta zeolites, as a result from the decomposition of furan rings. Furthermore, Beta–10 zeolite attained a smaller yield of EMF at this higher temperature. For ZSM5 zeolites, carbon balance values are similar to those found at 140 ºC, but EMF yields were close to 36%, at a 46% conversion. It is interesting to note that these conversion and EMF yield values are similar for the different ZSM5, despite their different acidity and aluminium content. This would suggest that ZSM5 materials may have suffered some deactivation, or some equilibrium may have been reached. Nevertheless, the activity of the FER–10 zeolite was still very limited. Therefore, the

difference between the activities of the catalysts are more easily observed at 140 °C, especially for the beta zeolites, where the conversion of HMF provides insights into the higher activity of the zeolites with higher aluminium content.

3.2. Glucose to EMF screening

Glucose is an aldose sugar, which could not be directly dehydrated to HMF, which is subsequently etherified into EMF. Instead, it is widely accepted that glucose needs first to isomerize to fructose, which takes place on basic or Lewis acid sites [41], before being dehydrated. On the other hand, it has been observed that, in the presence of Brønsted acid sites, hemiketalic monosaccharides, specially aldoses, can be etherified with alcohols to form stable ketals. In the case of glucose in ethanol, ethyl glucosides are formed, preferentially, instead of HMF or EMF [42]. However, in the case of ketoses, the protonic form of zeolites has strong Brønsted acid sites able to carry out the transformation of fructose to EMF.

As the zeolites in this work present both Lewis and Brønsted acid sites, they were studied for the one-pot transformation of glucose to EMF. Due to the greater difficulty for glucose conversion than for furan derivatives, reaction temperature was realized at 160 °C. Also, 0.15 g of glucose were used instead of 0.1 g of HMF, which is roughly equal number of moles of reactant (Fig. 4). The rest of conditions were kept constant. All zeolites were very active in the conversion of glucose in ethanol, with conversion values higher than 50%, and close to 100% for Beta zeolites with higher aluminum contents. In addition, EMF formation was only detected for Beta–16 and Beta–10. This mean that most of the converted glucose did not evolve to fructose, fructose derivatives, or furans. Instead, glucose was simply etherified in presence of strong Brønsted acid sites to form ethyl glucopyranosides and other ethyl glycosides. Ethyl glycosides were the major reaction products in the case of ZSM5 zeolites, FER–10 and Beta–96 (over 30% yield), the catalysts with a lower activity. Moreover, small quantities of HMF, furfural and ethyl levulinate were also detected. This correlates well with the Brønsted to Lewis acid sites ratios found by pyridine adsorption coupled to FTIR spectroscopy (pyr-FTIR) (Table 2, Fig. S5), since FER and ZSM5 catalysts showed basically only Brønsted acidity. Despite that ZSM5 zeolites with a high aluminum content presented a high concentration of octahedral Al species, pyr-FTIR analysis would indicate accessibility limitations to the Lewis acid sites, that could be associated to octahedral Al sites. It is important to note that, in spite of the Lewis acidity found by pyr-FTIR in the Beta–96 zeolite, this zeolite was unable to produce HMF or other furan derivatives from glucose. Nevertheless, Beta–10 and Beta–16 both possessed octahedral aluminum sites (Fig. S3), in contrast to Beta–95. Therefore, although the Beta–10 and Beta-16 had higher Brønsted/Lewis acidity than the zeolite Beta–95 (0.6, 0.6 and 0.16 respectively), the beta zeolites with higher aluminum content had stronger acid sites, as seen by NH_3-TPD. This suggests the importance of such sites for attaining a proper isomerization of glucose to fructose. The high glucoside and low EMF yields are in accordance with the previous statement, in which it was claimed that glucose required a higher reaction temperature due to the difficulty of the process. The slower transformation of glucose into furans is indeed a sign of the higher activation energy in the glucose to HMF transformation, where the key limiting steps of the reaction are found.

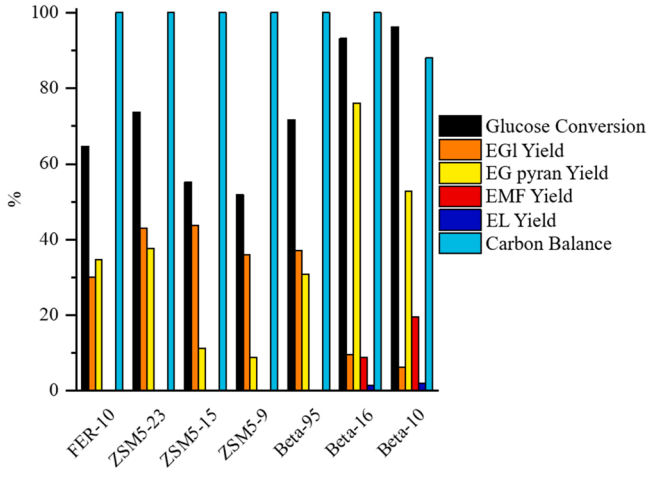

Fig. 4. Catalytic performance of different zeolites in glucose conversion in ethanol (EGl: Ethyl glycoside; EG pyran: Ethyl glycopyranosides; EL, Ethyl levulinate). (Experimental conditions: 0.15 g glucose, 0.05 g zeolite, 5 ml ethanol, 3 h, 160 °C).

3.3. Glucose to EMF study

As it was mentioned before, the best catalyst for the conversion of glucose into EMF was Beta–10 zeolite; therefore, for a better understanding of its catalytic behavior, the influence of reaction time was evaluated at three different temperatures: 140, 160 and 180 °C. Fig. 5 shows that glucose conversion was fast even at the lowest temperature assayed.

From the kinetic study realized at 140 °C (Fig. 5a), it can be inferred that glucose is first transformed rapidly into a variety of ethyl glycosides, that later isomerize to the more stable form of ethyl glucosides, particularly ethyl glucopyranosides. Carbon balance was maintained stable around 85%. In the first hour, glucopyranosides (27%) and other ethyl glycosides (48%) were the principal products in the reaction. EMF yield increased over time, until a maximum of 25% was achieved after 16 h. Ethyl levulinate (EL) and furfural yields remained always low at this reaction temperature. At 160 °C (Fig. 5b), ethyl glycosides were converted fast and, after 3 h, only 5% remained. An EMF yield of 24% was reached after 5 h, which was maintained mostly stable until 24 h, even though EMF yield suffered continuous rehydration under these conditions, as evidenced by EL production. EL yield rapidly increased after 7 h, attaining 15% after 24 h. Carbon balance decreased steadily, as well as ethyl glucopyranoside yield, meaning that EMF was being produced by the remaining sugars and being rehydrated to produce EL and humins at similar rates. At the highest temperature (180 °C) (Fig. 5c), ethyl glucopyranose yield decays rapidly, dehydrating to form EMF, whose yield was 28% after 3 h, which is higher than those values obtained at lower temperatures and longer reaction times. Once the hexoses present in the medium depleted, EMF yield decreased linearly with time. EL yield was highly favored at 180 °C, reaching a 31% yield after 16 h of reaction. Interestingly, reaction paths leading to furfural were seemingly promoted with temperature. At 180 °C, furfural yield rose steadily until a 15% was achieved.

3.4. Reaction pathway

^{13}C NMR was used to elucidate the reaction mechanism of these processes. Thus, for the identification of the reaction intermediates formed, the catalytic process was carried out at 140 °C, 5 ml of ethanol, 0.15 g of glucose and 0.05 g of Beta–10 zeolite, during 1, 3 and 24 h. The lowest temperature was employed to produce a higher amount of ethyl glycosides, which are rapidly converted at higher temperatures.

After 1 h, signals corresponding to unconverted glucose, in α- and β-pyranose forms (Gp α and Gp β, respectively), are detected at 92.0 and 95.8 ppm, respectively (Fig. S6). The kinetics products of etherification, that is, β-ethyl glucofuranose (EGf β) and α-ethylglucofuranose (EGf α) were observed at 107.7 and 101.9 ppm, respectively. At short reaction times, only small signals of ethyl glucopyranoses, α- and β- forms (EGp α and EGp β), could be seen at 97.8 and 101.8 ppm. It is important to point out that a signal assigned to β-ethylfructopyranoside (EFp β) appears at 98.0 ppm. After 3 h of reaction, ethyl glucofuranoses had almost disappeared from the solution, converted to more stable glucopyranoses.

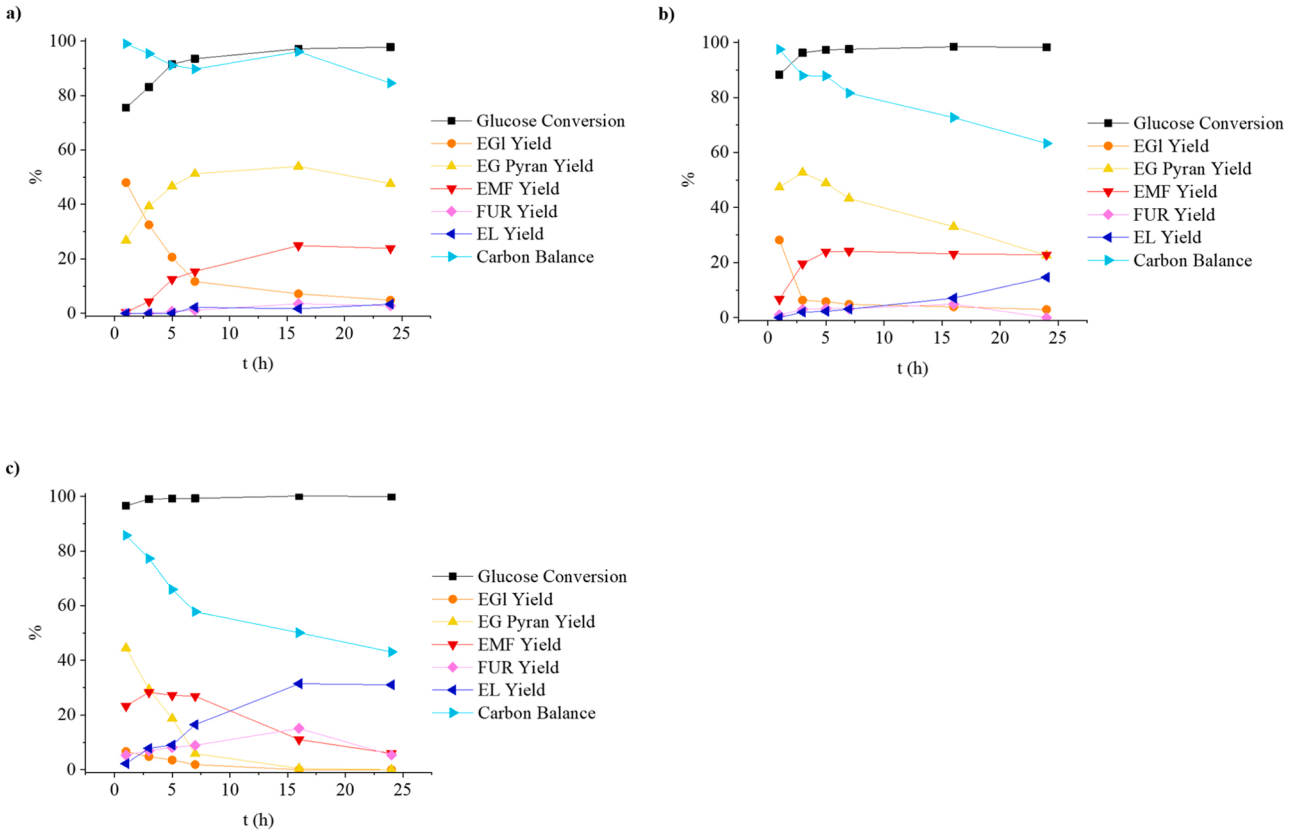

Fig. 5. Influence of reaction time using the Beta–10 zeolite at: a) 140 ºC, b) 160 ºC and c) 180 ºC (EGl: Ethyl glycoside; EG pyran: Ethyl glycopyranosides; EL, Ethyl levulinate) (Experimental conditions: 0.15 g glucose, 0.05 g catalyst and 5 ml ethanol).

Still, a small quantity of ethyl-β-fructopyranoside was detected after this time. However, most signals disappeared after 24 h of reaction, and all remaining glucose was found in the form of ethyl glucopyranosides.

Therefore, we can depict, with the data available, the mechanistic pathways by which glucose is transformed into EMF (Fig. 6). Firstly, glucose is etherified rapidly to ethyl glucofuranosides. These compounds are labile and quickly transform to the more stable ethyl glucopyranose, or returns to the non-etherified form, as an equilibrium. The etherified forms of glucose cannot produce fructose or ethyl fructosides, as they have their carbonyl group protected, nor can they undergo an intramolecular hydrogen transfer to form the ketose form. Therefore, all transformations from glucose to fructose must take place from the non-etherified glucose, in equilibrium with the etherified forms. On one hand, ethyl-β-fructopyranose is the most abundant form of fructose observed in this study, and the only one that could be assigned by ^{13}C NMR experiment. The furanose form of fructose should be attained to provide the proper carbon skeleton of 5-hydroxymethylfurfural. After the elimination of three water molecules, HMF is formed, that is subsequently etherified into EMF.

Regarding the mechanism of production of furfural from hexoses, different pathways have been proposed in the literature to explain the formation of this C5 compound from C6 sugars. Thus, Cui et al. established that fructose in the open form undergoes C-C bond cleavage, resulting in formaldehyde and a C5 sugar that would dehydrate to produce furfural [43]. Using Beta zeolite in γ-butyrolactone 5 wt% in water, they could produce 63% furfural yield from fructose after 1 h at 150 ºC and 2 MPa of N_2. More recently, Asakawa et al. found a relationship between the proton affinity of solvents and the selectivity towards furfural [44]. When fructose dehydrates, the resulting intermediate, after losing two water molecules, is susceptible to lose a third molecule to originate HMF. But this intermediate may instead lose a formaldehyde molecule assisted by basic solvents to be transformed into furfural. They supported their findings with DFT calculations, and isotopic labeling, that confirmed that the anomeric carbon of glucose is present in furfural and should not be if it was produced by C-C bond cleavage in the open chain form of fructose.

3.5. Utilization of co-solvents

So far, the production of EMF from glucose in ethanol media has been studied. However, previous works have pointed out that the application of co-solvents can have a beneficial effect on the selectivity of the process towards the formation of furans. Among the most frequently employed solvents, GVL [45,46] and THF [19,45,47] can be found.

Thus, polar aprotic solvents have been used to improve furan yields from fructose and glucose. Hence, in the present work, GVL, THF and MIBK were employed to study the potential application of these co-solvents to improve EMF production in the presence of ethanol (Fig. 7a). The results of the experiment without co-solvent are also showed for comparison.

The use of GVL and THF as co-solvents gave rise to important differences in the selectivity pattern. THF, and specially GVL, favour the formation of furfural (yields of 8% and 9%, respectively), agreeing well with the conclusion drawn by Asakawa et al. [44]. GVL is more basic than THF, and both more than ethanol, so they can play a more important role in the deformilation of the fructose intermediate into furfural, instead of helping in the dehydration of the aforementioned intermediate [45]. However, they had little or not positive effect on EMF yield, with the GVL and THF experiments originating 16% and 20% EMF yield, respectively, similar to the value attained with pure ethanol (20% EMF yield), which contrasts with the results obtained by other authors [19,48,49]. Therefore, although the use of GVL or THF did not have a positive effect on the selectivity towards EMF, higher total furan yields (HMF plus EMF plus furfural) were achieved by using the co-solvents

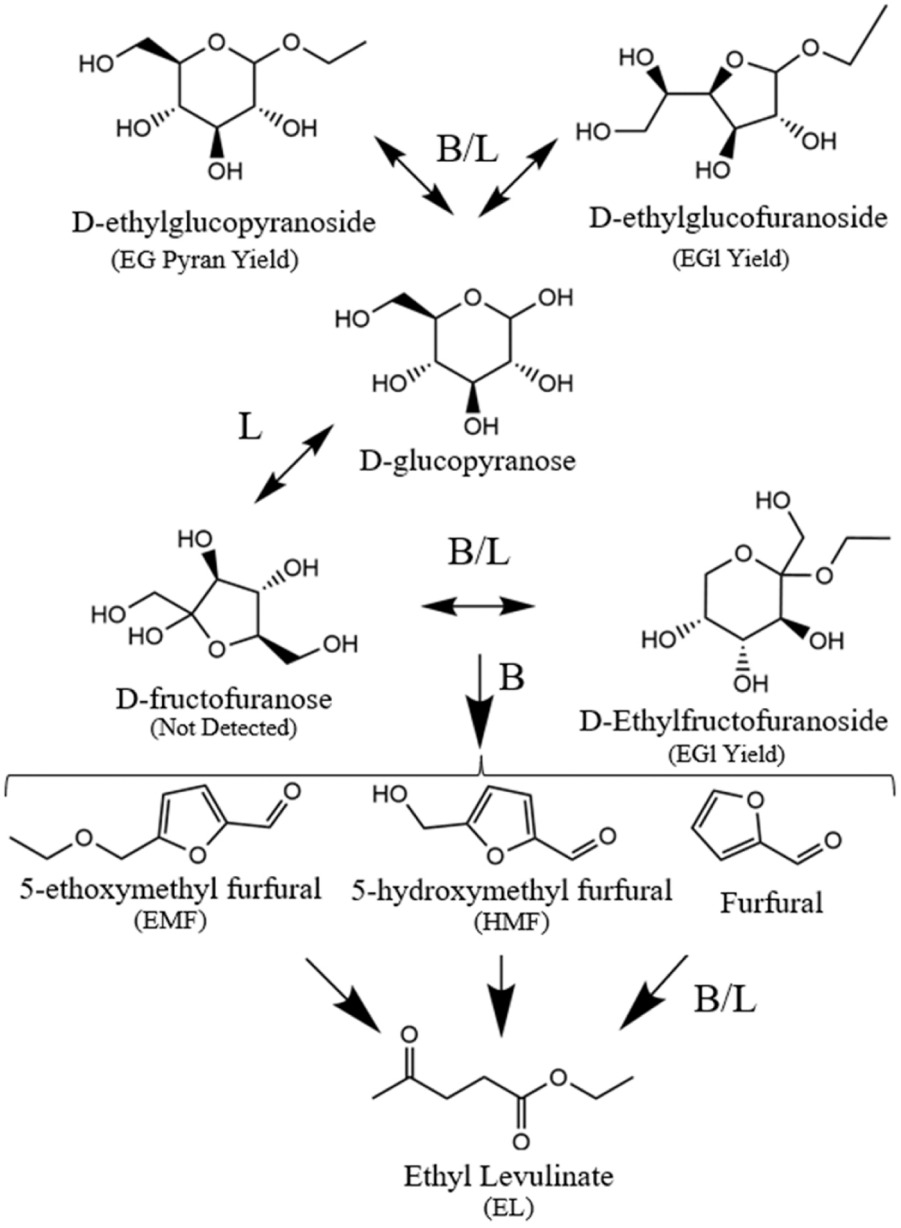

Fig. 6. Proposed mechanistic pathways for glucose conversion in ethanol. B: Brønsted acid sites. L: Lewis acid sites.

instead of pure ethanol. At the same time, a significant amount of non-etherified HMF was found. The reason behind the high quantities of non-etherified HMF is probably analogue to the actuation mechanism of DMSO, as described by Mushrif et al. [50]. The co-solvent molecules can solvate the HMF molecule, causing an increase in the protonation energy. Consequently, HMF etherification slows down. Despite the absence of improvement in EMF yield, the use of GVL and THF as cosolvent could favour the production of valuable furans from biomass derived hexoses (Fig. 7a). Nevertheless, both co-solvents, GVL and THF, demonstrated to be unstable under these experimental conditions. It is noteworthy that an immiscible phase appeared when mixed with water. It was confirmed, in absence of glucose, that the decomposition of GVL in the presence of Beta–10 zeolite (Fig. S7) can take place at temperatures as low as 120 ºC. As a consequence, the instability of GVL and THF should be considered when utilising them to improve the furan yields from saccharides, as well as the cost of purification of the secondary products coming from the co-solvent degradation, so their replacement must be considered. The use of MIBK, as a cosolvent, resulted beneficial for both the EMF (22%) and HMF (10%) yields respect to the values obtained using only ethanol. MIBK has already been tested as cosolvent for this process, and Xin et al. already observed a positive effect on the EMF production, from glucose and ethanol, when MIBK was used together with ethanol and water. A 13.2% EMF yield was obtained, together with a 25% HMF yield [25].

The addition of water as a cosolvent was also tested, since it has been reported that the presence of water favours the isomerization of glucose into fructose, a necessary step for the production of HMF from glucose. Yang et al. utilized ethanol-water mixtures for the production of furans [51]. Using $AlCl_3$ as acid catalyst, it was demonstrated that the addition of small quantities of water (10 wt%) improved the production of furans. Thus, in the absence of water, the total furan yield (HMF plus EMF) was 44%, while it was 58% in the presence of a 10 wt% of water. However, a high amount of water is detrimental for the production of furans, and the etherification of glucose is also severely hindered. In the present study, although a fructose yield of 15% was obtained, only minimal HMF yield was attained. Low furan yields and high glucose and fructose quantities detected after 3 h, at 160 ºC, are the result of very disfavoured dehydration conditions in aqueous media.

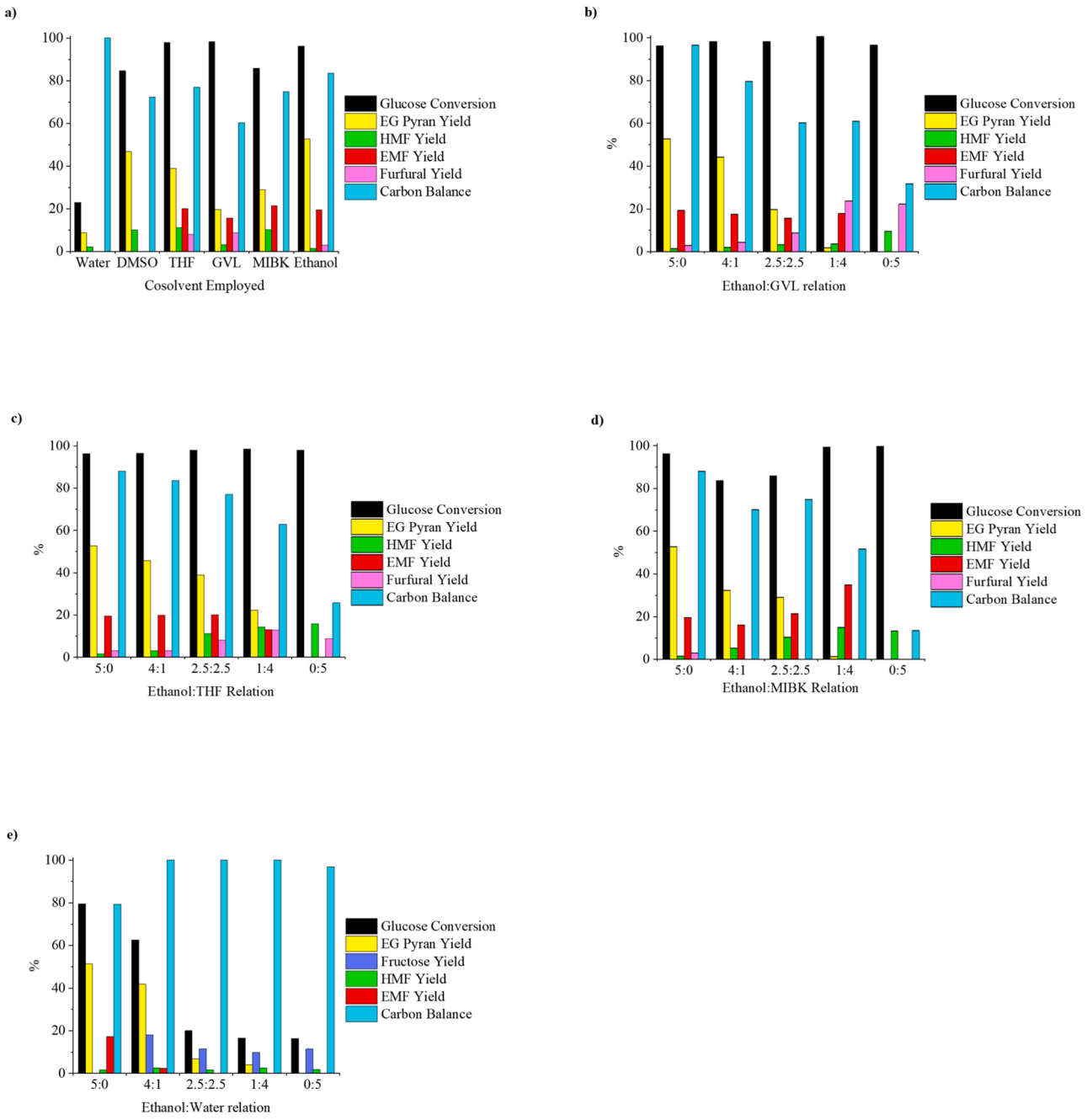

Fig. 7. Influence of different ethanol:co-solvent mixtures on EMF production from glucose: a) 2.5 ml co-solvent and 2.5 ml ethanol, b) ethanol:GVL mixtures, c) ethanol:THF mixtures, d) ethanol:water mixtures, and e) ethanol:MIBK mixtures (Experimental conditions: 0.15 g glucose; 0.05 g Beta–10 zeolite, 5 ml total solvent, 160 °C and 3 h).

It was deemed that, at least under the experimental conditions used in the present work, the addition of GVL, THF, MIBK and water to the reaction media (ethanol) could provide interesting results. Thus, different ethanol:co-solvent volume ratios were evaluated. In the case of GVL (Fig. 7b), EMF yields are very similar, achieving a 18% EMF yield, regardless the ethanol:GVL volume ratio. However, HMF yield increased as more GVL was added, and finally rose to 10% yield with pure GVL. Furfural yield experienced a sharp rise as GVL proportion increased, changing from a 3–24% yield when the ethanol:GVL ratio varied from 5:0–1:4. A total furan yield of 45% was detected at 1:4 ethanol:GVL ratio. However, furfural yield barely changed after removing ethanol entirely from the medium, and a 22% furfural yield was obtained when the reaction was carried out in pure GVL. It is interesting to note that the presence of ethanol is a key factor for the formation of HMF. Thus, in the absence of ethanol, no EMF was detected, but HMF yield was much lower than expected. This leads to the conclusion than ethanol intervenes in the dehydration of fructose and stabilizes the intermediate produced in the pathway to produce HMF. When ethanol is absent, the intermediate evolves producing unwanted polymerization products.

When THF was employed as co-solvent (Fig. 7c), the formation of glucopyranosides was less hindered as the THF proportion increased respect to the GVL study, and significant ethyl glucopyranosides formation was still found at an ethanol:THF volume ratio of 1:4. Similarly to what was observed with GVL, carbon balance was negatively affected by the addition of THF. The less ethanol the reactor contained, the higher was the HMF yield. HMF etherification seemed to be impeded at

high THF loadings, leading to lower EMF yields, something that has not been observed when GVL was utilised. While EMF yield remained constant, HMF yield increased notably. On the other hand, furfural yield was highest when the relation 1:4 was employed.

Therefore, although total yield of furans produced from glucose is increased when GVL of THF is increased, the final EMF yield was not improved. This was changed when MIBK was used as cosolvent. Interestingly, no furfural was detected when MIBK was utilized as cosolvent (Fig. 7d). Moreover, the maximum EMF yield (39%) was attained for a 1:4 ethanol:MIBK volume ratio, together with a 4% HMF yield. This is the result of a simultaneous limitation of the deformilation pathway in the formation of furfural from the saccharide reactants and the promotion of dehydration effects in the hydrophobic media offered by the organic solvent. The final EMF yield was observed to reach 39%. By using pure MIBK, EMF was not detected, whereas a 13% HMF yield was produced. In the latter case, the carbon balance was so low because of the insolubility of glucose in MIBK.

In the case of water as a cosolvent (Fig. 7e), it was noteworthy that the fructose yield increased with the ethanol content. Fructose yield, from the isomerization of glucose, was low when the reaction was carried out in pure water (11% yield). With increasing ethanol content, fructose isomerization was favoured until a maximum yield (18%) was attained with an ethanol:water of 4:1. However, in pure ethanol (ethanol:water ratio of 5:0), fructose is missing from the analysis. Indeed, Van der Graaff determined the adsorption enthalpy of THF, water and ethanol on the acid sites of a Sn-beta zeolite to be − 100, − 58 and − 43 KJ·mol^{-1} [52]. That means that the adsorption of THF or water on active centres of zeolite is more favourable than the adsorption of a glucose molecule (−48 KJ·mol^{-1}), thus suggesting that the reaction is slowed down by the presence of water, and it should be affected in an even stronger way when THF is utilized instead. This contrasts with our results, where THF does not seem to hinder the transformation of glucose due to displacement of glucose from the Lewis acid sites. On the other hand, in all cases, furan yields are very low in the presence of water, with a maximum HMF yield of 4%, while EMF could not be detected with ethanol:water ratios lower than 4:1. When water is absent, the total furan yield, or the combination of EMF and HMF, is maximum. Consequently, it can be deduced that, in an aqueous environment, fructose is stabilized, and dehydration happens at a very slow rate. Kuster et al. reported that the formation of enediol from fructose requires the desolvation of the acidic proton interacting with fructose [53]. This is facilitated when water is absent from the media, and it would explain why fructose could not be detected when water is not present, due to stronger interaction between the fructose moiety and the acidic proton. When water content falls below a threshold, the fructose moiety becomes highly reactive in the ethanol media and dehydrates readily. It is also interesting to point out that ethyl glucosides require at least four-fifths of the solvent to be ethanol to become a major product. Also, carbon balance was improved in the presence of water.

Thus, the use of co-solvents is indeed useful to improve the yield of furan-based compounds (EMF, furfural and HMF) obtained from the treatment of glucose in ethanol. For the most efficient ethanol:co-solvent volume ratio, in the case of GVL, THF and MIBK, the time of the reaction was optimized (Fig. 8). It was found that, with GVL, a total furan yield of 51% could be achieved at 160 °C, after 5 h, with 22% and 24% of EMF and furfural yields, respectively. When THF was used instead, an EMF and furfural yields of 26% and 7%, respectively, were achieved at 160 °C, after 24 h. It is noteworthy that, in both cases, EMF and furfural yields are stable under the experimental conditions used, as no downward trend is observable in any case. On the other hand, the use of the optimum ethanol:MIBK volume ratio (1:4) provided the best EMF yield. These results were likely related to the fact that the formation of furfural

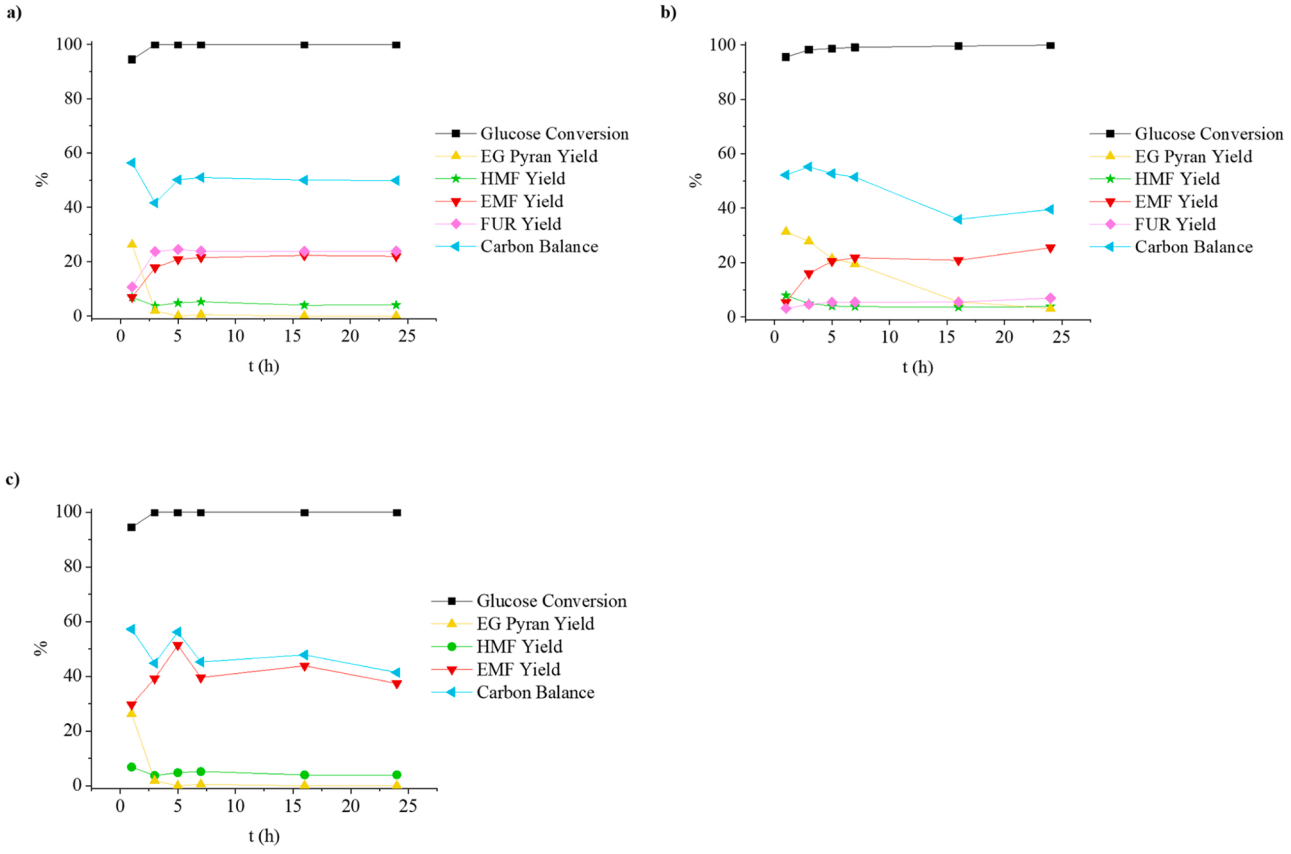

Fig. 8. Effect of reaction time on the etherification of glucose with ethanol using the optimum ethanol:co-solvent volume ratio: a) GVL (1 ml Ethanol, 4 ml GVL), b) THF (2.5 ml ethanol, 2.5 ml THF), and c) MIBK (1 ml ethanol, 4 ml MIBK). (Experimental conditions: 0.15 g glucose, 0.05 g Beta–10, 160°C).

was inhibited under these experimental conditions. The result is up to 51% EMF yield, after 5 h of reaction at 160 ºC.

3.6. Reuse of catalyst

The reutilization of the catalyst was carried out under the optimum conditions of 5 h of reaction, with 4 ml of MIBK and 1 ml of ethanol. After reaction, the catalyst was left to precipitate to the bottom of the reactor, before extracting the solvent. After that, more solvent and glucose were added to the reactor, without any washing pretreatment. The reaction (Fig. 9) shows decreased activity in each consecutive cycle. EMF yield changes from 51% in the first cycle to 40% in the second, and 34% in the third. The constant increase in yield of the intermediates also denotes consecutive activity loss. After the 4 reuses, the catalyst was dried at 70 ºC overnight before submitting it for analysis. By XPS, a 58% of the analyzed surface was determined to be carbon. When compared with the adventitious carbon that was found on the pristine zeolite (15%), it is highlighted the extension of carbon deposition on the catalyst surface. By thermogravimetric analysis (Fig. S8) two noticeable exothermic peaks were detected at 345 and 490 ºC, being associated with burning of organic compounds. 60% total mass loss was found by thermogravimetric data after exposure at 600 ºC, which means that there is a high concentration of carbon residues on the reactor after 4 consecutive tests.

4. Conclusions

The catalytic performance of different zeolites has been studied for the valorisation of glucose into biofuels and platform molecules, under batch conditions. The results obtained have demonstrated that the textural properties strongly influence the catalytic activity in etherification processes, much more than the aluminium content (acid properties). At 140 ºC, zeolites with narrower micropore size, such as ferrierite and ZSM5, produced low EMF yields (2 and 17%, respectively) from HMF, while Beta zeolites, with wider pores, provided a good EMF yield (77% with Beta–10 zeolite). In addition, it has been demonstrated that, for the ZSM5 and Beta zeolites, the overall activity correlates very well with the aluminium content.

The Beta–10 zeolite produced the best results in the glucose dehydration and etherification processes compared to the rest of the zeolites studied. Brønsted acid sites catalyse the etherification of sugars to their etherified forms, while it is known that Lewis acidity is required for the transformation of glucose into fructose, which can proceed with the dehydration through the intervention of Brønsted acid sites. This same type for acid later allows the etherification of HMF into the final product EMF. Beta zeolites are able to catalyse the process thanks to both the protonic acid sites, that appear when aluminium substitutes silicon in the structure, and the octahedral extraframework centres, that provide Lewis acid sites. The influence of reaction time employing the Beta–10 zeolite provided a maximum EMF yield of 24%, at 160 ºC after 7 h, and was further improved after increasing the temperature to 180 ºC, whereas a 28% EMF yield was obtained after 3 h. Moreover, ^{13}C NMR analysis suggests that glucose is isomerized and etherified into different compounds, such as ethylglucofuranosides and the key intermediate ethyl-β-fructopyranose, but all the products tend to adopt the thermodynamically more stable form of glucopyranosides, where the reaction stalls.

In order to optimize our results and gain insights into the influence of co-solvents in the catalytic process, water, GVL, THF and MIBK were employed together with ethanol. Small quantities of water were found to exert a positive effect on the formation of fructose, but severely hindered dehydration, and furans were formed in very small quantities. However, GVL and THF, as co-solvents, had a very positive effect on the total furan yield (HMF + EMF + Furfural). EMF yield was barely affected by the presence of the co-solvent, but HMF and, especially, furfural yields were improved. Unlike with the other tested cosolvents, the use of MIBK supressed the deformilation. In consequence, furfural was not originated and the selectivity towards EMF was increased substantially. The ethanol:MIBK ratio of 1:4 was the optimal for the production of EMF, up to a 51% EMF yield after only 5 h of reaction.

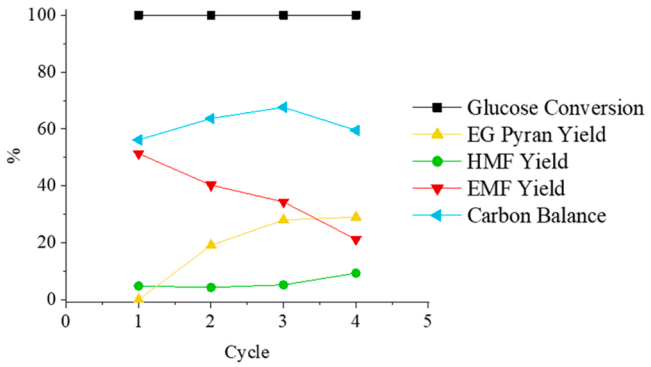

Fig. 9. Reuse of the catalyst Beta–10 in the optimum reaction conditions (1 ml ethanol, 4 ml MIBK, 0.15 g glucose, 0.05 g catalyst, 5 h, 160 ºC).

Finally, the reutilization of the catalyst Beta–10 has been studied under the optimum conditions achieved in this work. However, it was found that the zeolite experienced activity loss overtime, and the yield decreased from 51% in the first cycle to 21% after 4 reuses. The activity loss of the catalyst has been explained by the high amount of carbon deposits found on the catalyst surface, that hinders the accessibility to catalytically active sites.

CRediT authorship contribution statement

Benjamín Torres-Olea: Investigation, Formal analysis, Writing – review & editing. **Antonio Pérez Merchán**: Investigation. **Paula Díaz-Maizkurrena** Investigation. **Jesús M. Requies**: Investigation, Funding acquisition. **Ramón Moreno-Tost:** Writing – review & editing, Supervision, Funding acquisition. **Juan Antonio Cecilia:** Investigation. **Cristina García-Sancho:** Conceptualization, Investigation, Writing – review & editing, Supervision. **Pedro Maireles-Torres:** Conceptualization, Resources, Writing – review & editing, Funding acquisition, Project administration, Supervision.

Declaration of Competing Interest

The authors declare the following financial interests/personal relationships which may be considered as potential competing interests: All authors reports financial support was provided by Spanish Ministry of Science and Innovation (PID2021–122736OB-C42 and PID2021–122736OB-C43). All authors reports financial support was provided by FEDER (European Union) funds (PID2021–122736OB-C42, P20–00375, UMA20-FEDERJA-088). B. Torres Olea reports financial support was provided by Ministerio de Universidades for his predoctoral contract FPU20–02334.

Data availability

Data will be made available on request.

Acknowledgments

Funding: This research was funded by Spanish Ministry of Science and Innovation (PID2021–122736OB-C42 and PID2021–122736OB-C43), FEDER (European Union) funds (PID2021–122736OB-C42, P20–00375, UMA20-FEDERJA-088) and B. Torres-Olea thanks *Ministerio de Universidades* for his predoctoral contract (FPU20/02334). Moreover, authors want to thank the funding for open access charge to Universidad de Málaga / CBUA.

Appendix A. Supporting information

Supplementary data associated with this article can be found in the online version at doi:10.1016/j.cattod.2023.114439.

References

[1] X. Tang, J. Wei, N. Ding, Y. Sun, X. Zeng, L. Hu, S. Liu, T. Lei, L. Lin, Chemoselective hydrogenation of biomass derived 5-hydroxymethylfurfural to diols: key intermediates for sustainable chemicals, materials and fuels, Renew. Sustain. Energy Rev. 77 (2017) 287–296, https://doi.org/10.1016/j.rser.2017.04.013.

[2] K. Vikanova, E. Redina, G. Kapustin, M. Chernova, O. Tkachenko, V. Nissenbaum, L. Kustov, Advanced room-temperature synthesis of 2,5-Bis(hydroxymethyl)furan-A Monomer for Biopolymers-From 5-Hydroxymethylfurfural, ACS Sustain Chem. Eng. 9 (2021) 1161–1171, https://doi.org/10.1021/acssuschemeng.0c06560.

[3] S. Alipour, H. Omidvarborna, D.S. Kim, A review on synthesis of alkoxymethyl furfural, a biofuel candidate, Renew. Sustain. Energy Rev. 71 (2017) 908–926, https://doi.org/10.1016/j.rser.2016.12.118.

[4] A. Bohre, S. Dutta, B. Saha, M.M. Abu-Omar, Upgrading furfurals to drop-in biofuels: an overview, ACS Sustain Chem. Eng. 3 (2015) 1263–1277, https://doi.org/10.1021/acssuschemeng.5b00271.

[5] Y. Yang, M.M. Abu-Omar, C. Hu, Heteropolyacid catalyzed conversion of fructose, sucrose, and inulin to 5-ethoxymethylfurfural, a liquid biofuel candidate, Appl. Energy 99 (2012) 80–84, https://doi.org/10.1016/j.apenergy.2012.04.049.

[6] H. Wang, T. Deng, Y. Wang, Y. Qi, X. Hou, Y. Zhu, Efficient catalytic system for the conversion of fructose into 5-ethoxymethylfurfural, Bioresour. Technol. 136 (2013) 394–400, https://doi.org/10.1016/j.biortech.2013.02.110.

[7] J. Zhang, K. Dong, W. Luo, H. Guan, Catalytic upgrading of carbohydrates into 5-ethoxymethylfurfural using SO3H functionalized hyper-cross-linked polymer based carbonaceous materials, Fuel 234 (2018) 664–673, https://doi.org/10.1016/j.fuel.2018.07.060.

[8] L. Zhang, Y. Zhu, L. Tian, Y. He, H. Wang, F. Deng, One-pot alcoholysis of carbohydrates to biofuel 5-ethoxymethylfufural and 5-methoxymethylfufural via a sulfonic porous polymer, Fuel Process. Technol. 193 (2019) 39–47, https://doi.org/10.1016/j.fuproc.2019.05.001.

[9] O.H. Pardo Cuervo, S.P. Simeonov, A.F. Peixoto, M.D. Popova, H.I. Lazarova, G. P. Romanelli, J.J. Martínez, C. Freire, C.A.M. Afonso, Efficient continuous production of the biofuel additive 5-(t-Butoxymethyl) furfural from 5-hydroxymethylfurfural, Energy Technol. 7 (2019) 1–9, https://doi.org/10.1002/ente.201900780.

[10] E. Mahmoud, Glucose conversion to furans in alcohols catalyzed by lewis acidic beta zeolites and brønsted acidic resins, ChemistrySelect 2 (2017) 10336–10339, https://doi.org/10.1002/slct.201701815.

[11] C. Tao, L. Peng, J. Zhang, L. He, Al-modified heteropolyacid facilitates alkyl levulinate production from cellulose and lignocellulosic biomass: kinetics and mechanism studies, Fuel Process. Technol. 213 (2021), 106709, https://doi.org/10.1016/j.fuproc.2020.106709.

[12] H.S. Kim, G.T. Jeong, Valorization of galactose into levulinic acid via acid catalysis, Korean J. Chem. Eng. 35 (2018) 2232–2240, https://doi.org/10.1007/s11814-018-0126-5.

[13] A. Bohre, S. Dutta, B. Saha, M.M. Abu-Omar, Upgrading furfurals to drop-in biofuels: an overview, ACS Sustain Chem. Eng. 3 (2015) 1263–1277, https://doi.org/10.1021/acssuschemeng.5b00271.

[14] Z. Wang, Q. Chen, Conversion of 5-hydroxymethylfurfural into 5-ethoxymethylfurfural and ethyl levulinate catalyzed by MOF-based heteropolyacid materials, Green. Chem. 18 (2016) 5884–5889, https://doi.org/10.1039/c6gc01206j.

[15] B. Torres-Olea, I. Fúnez-Núñez, C. García-Sancho, J.A. Cecilia, R. Moreno-Tost, P. Maireles-Torres, Influence of Lewis and Brønsted acid catalysts in the transformation of hexoses into 5-ethoxymethylfurfural, Renew. Energy 207 (2023) 588–600, https://doi.org/10.1016/j.renene.2023.03.036.

[16] G. Morales, M. Paniagua, J.A. Melero, J. Iglesias, Efficient production of 5-ethoxymethylfurfural from fructose by sulfonic mesostructured silica using DMSO as co-solvent, Catal. Today 279 (2017) 305–316, https://doi.org/10.1016/j.cattod.2016.02.016.

[17] R. Zhong, F. Yu, W. Schutyser, Y. Liao, F. de Clippel, L. Peng, B.F. Sels, Acidic mesostructured silica-carbon nanocomposite catalysts for biofuels and chemicals synthesis from sugars in alcoholic solutions, Appl. Catal. B 206 (2017) 74–88, https://doi.org/10.1016/j.apcatb.2016.12.053.

[18] G. Xu, S. Zhang, Z. Zheng, C. Wang, S. Wang, H. Tao, Direct conversion of fructose to 5-ethoxymethyl-furfural catalyzed by ultrastable Y zeolite, Bioresources 15 (2020) 3621–3635, https://doi.org/10.15376/biores.15.2.3621-3635.

[19] B. Chen, G. Xu, Z. Zheng, D. Wang, C. Zou, C. Chang, Efficient conversion of corn stover into 5-ethoxymethylfurfural catalyzed by zeolite USY in ethanol/THF medium, Ind. Crops Prod. 129 (2019) 503–511, https://doi.org/10.1016/j.indcrop.2018.12.027.

[20] E. Mahmoud, Glucose conversion to furans in alcohols catalyzed by Lewis acidic beta zeolites and brønsted acidic resins, ChemistrySelect 2 (2017) 10336–10339, https://doi.org/10.1002/slct.201701815.

[21] Z. Zheng, C. Wang, Y. Chen, S. Wang, Q. Guo, C. Chang, H. Tao, G. Xu, One-pot efficient conversion of glucose into biofuel 5-ethoxymethylfurfural catalyzed by zeolite solid catalyst, Biomass-.-. Convers. Biorefin (2021), https://doi.org/10.1007/s13399-021-01660-1.

[22] H. Guo, X. Qi, Y. Hiraga, T.M. Aida, R.L. Smith, Efficient conversion of fructose into 5-ethoxymethylfurfural with hydrogen sulfate ionic liquids as co-solvent and catalyst, Chem. Eng. J. 314 (2017) 508–514, https://doi.org/10.1016/j.cej.2016.12.008.

[23] B. Liu, Z. Zhang, K. Huang, Z. Fang, Efficient conversion of carbohydrates into 5-ethoxymethylfurfural in ethanol catalyzed by AlCl3, Fuel 113 (2013) 625–631, https://doi.org/10.1016/j.fuel.2013.06.015.

[24] J. Liu, Y. Tang, K. Wu, C. Bi, Q. Cui, Conversion of fructose into 5-hydroxymethylfurfural (HMF) and its derivatives promoted by inorganic salt in alcohol, Carbohydr. Res 350 (2012) 20–24, https://doi.org/10.1016/j.carres.2011.12.006.

[25] H. Xin, T. Zhang, W. Li, M. Su, S. Li, Q. Shao, L. Ma, Dehydration of glucose to 5-hydroxymethylfurfural and 5-ethoxymethylfurfural by combining Lewis and Brønsted acid, RSC Adv. 7 (2017) 41546–41551, https://doi.org/10.1039/c7ra07684c.

[26] I. Langmuir, The adsorption of gases on plane surfaces of glass, mica and platinum, J. Am. Chem. Soc. 40 (1918) 1361–1403, https://doi.org/10.1021/ja02242a004.

[27] J. Landers, G.Y. Gor, A.V. Neimark, Density functional theory methods for characterization of porous materials, Colloids Surf. A Physicochem Eng. Asp. 437 (2013) 3–32, https://doi.org/10.1016/j.colsurfa.2013.01.007.

[28] R.S. Mikhail, S. Brunauer, E.E. Bodor, Investigations of a complete pore structure analysis, J. Colloid Interface Sci. 26 (1968) 45–53, https://doi.org/10.1016/0021-9797(68)90270-1.

[29] C.A. Emeis, Determination of integrated molar extinction coefficients for infrared absorption bands of pyridine adsorbed on solid acid catalysts, J. Catal. 141 (1993) 347–354, https://doi.org/10.1006/jcat.1993.1145.

[30] M. Thommes, K. Kaneko, A.V. Neimark, J.P. Olivier, F. Rodriguez-Reinoso, J. Rouquerol, K.S.W. Sing, Physisorption of gases, with special reference to the evaluation of surface area and pore size distribution (IUPAC Technical Report), Pure Appl. Chem. 87 (2015) 1051–1069, https://doi.org/10.1515/pac-2014-1117.

[31] I. Agirrezabal-Telleria, I. Gandarias, P.L. Arias, Heterogeneous acid-catalysts for the production of furan-derived compounds (furfural and hydroxymethylfurfural) from renewable carbohydrates: a review, Catal. Today 234 (2014) 42–58, https://doi.org/10.1016/j.cattod.2013.11.027.

[32] L. Hu, Z. Wu, Y. Jiang, X. Wang, A. He, J. Song, J. Xu, S. Zhou, Y. Zhao, J. Xu, Recent advances in catalytic and autocatalytic production of biomass-derived 5-hydroxymethylfurfural, Renew. Sustain. Energy Rev. 134 (2020), 110317, https://doi.org/10.1016/j.rser.2020.110317.

[33] S.M. Maier, A. Jentys, J.A. Lercher, Steaming of zeolite BEA and its effect on acidity: a comparative NMR and IR spectroscopic study, J. Phys. Chem. C. 115 (2011) 8005–8013, https://doi.org/10.1021/jp108338g.

[34] C. Lenardi, P. Piseri, V. Briois, C.E. Bottani, A.Li Bassi, P. Milani, Near-edge X-ray absorption fine structure and Raman characterization of amorphous and nanostructured carbon films, J. Appl. Phys. 85 (1999) 7159–7167, https://doi.org/10.1063/1.370527.

[35] D. Fischer, W.R. Caseri, G. Hähner, Orientation and electronic structure of ion exchanged dye molecules on mica: An x-ray absorption study, J. Colloid Interface Sci. 198 (1998) 337–346, https://doi.org/10.1006/jcis.1997.5296.

[36] A. Nylund, I. Olefjord, Surface analysis of oxidized aluminium. 1. Hydration of Al2O3 and decomposition of Al(OH)3 in a vacuum as studied by ESCA, Surf. Interface Anal. 21 (1994) 283–289, https://doi.org/10.1002/sia.740210504.

[37] T.L. Barr, The nature of the relative bonding chemistry in zeolites: An XPS study, Zeolites 10 (1990) 760–765, https://doi.org/10.1016/0144-2449(90)90058-Y.

[38] J.P. Rivière, Y. Pacaud, M. Cahoreau, Spectroscopic studies of BN films deposited by dynamic ion mixing, Thin Solid Films 227 (1993) 44–53, https://doi.org/10.1016/0040-6090(93)90185-R.

[39] M.C. Allen, A.J. Hoffman, T.W. Liu, M.S. Webber, D. Hibbitts, T.J. Schwartz, Highly Selective Cross-Etherification of 5-Hydroxymethylfurfural with Ethanol, ACS Catal. 10 (2020) 6771–6785, https://doi.org/10.1021/acscatal.0c01328.

[40] Ch Baerlocher, L.B. McCusker, Database of Zeolite Structures, (2022).

[41] V. Choudhary, S.H. Mushrif, C. Ho, A. Anderko, V. Nikolakis, N.S. Marinkovic, A. I. Frenkel, S.I. Sandler, D.G. Vlachos, Insights into the interplay of lewis and Brønsted acid catalysts in glucose and fructose conversion to 5-(hydroxymethyl) furfural and levulinic acid in aqueous media, J. Am. Chem. Soc. 135 (2013) 3997–4006, https://doi.org/10.1021/ja3122763.

[42] H. Li, S. Saravanamurugan, S. Yang, A. Riisager, Direct transformation of carbohydrates to the biofuel 5-ethoxymethylfurfural by solid acid catalysts, Green. Chem. 18 (2016) 726–734, https://doi.org/10.1039/c5gc01043h.

[43] J. Cui, J. Tan, T. Deng, X. Cui, Y. Zhu, Y. Li, Conversion of carbohydrates to furfural via selective cleavage of the carbon-carbon bond: the cooperative effects of zeolite and solvent, Green. Chem. 18 (2016) 1619–1624, https://doi.org/10.1039/c5gc01948f.

[44] M. Asakawa, A. Shrotri, H. Kobayashi, A. Fukuoka, Solvent basicity controlled deformylation for the formation of furfural from glucose and fructose, Green. Chem. 21 (2019) 6146–6153, https://doi.org/10.1039/c9gc02600b.

[45] H. Guo, A. Duereh, Y. Su, E.J.M. Hensen, X. Qi, R.L. Smith, Mechanistic role of protonated polar additives in ethanol for selective transformation of biomass-related compounds, Appl. Catal. B 264 (2020), https://doi.org/10.1016/j.apcatb.2019.118509.

[46] X. Jia, I.K.M. Yu, D.C.W. Tsang, A.C.K. Yip, Functionalized zeolite-solvent catalytic systems for microwave-assisted dehydration of fructose to 5-hydroxymethylfurfural, Microporous Mesoporous Mater. 284 (2019) 43–52, https://doi.org/10.1016/j.micromeso.2019.04.022.

[47] E. Nikolla, Y. Román-Leshkov, M. Moliner, M.E. Davis, One-pot" synthesis of 5-(hydroxymethyl)furfural from carbohydrates using tin-beta zeolite, ACS Catal. 1 (2011) 408–410, https://doi.org/10.1021/cs2000544.

[48] X. Yu, X. Gao, L. Peng, L. He, J. Zhang, Intensified 5-ethoxymethylfurfural production from biomass components over aluminum-based mixed-acid catalyst in Co-solvent medium, ChemistrySelect 3 (2018) 13391–13399, https://doi.org/10.1002/slct.201803059.
[49] Y.Y. Bai, S. Su, S. Wang, B. Wang, R.C. Sun, G. Song, L.P. Xiao, Catalytic conversion of carbohydrates into 5-ethoxymethylfurfural by a magnetic solid acid using γ-valerolactone as a Co-solvent, Energy Technol. 6 (2018) 1951–1958, https://doi.org/10.1002/ente.201800090.
[50] S.H. Mushrif, S. Caratzoulas, D.G. Vlachos, Understanding solvent effects in the selective conversion of fructose to 5-hydroxymethyl-furfural: A molecular dynamics investigation, Phys. Chem. Chem. Phys. 14 (2012) 2637–2644, https://doi.org/10.1039/c2cp22694d.
[51] Y. Yang, C. Hu, M.M. Abu-Omar, Conversion of glucose into furans in the presence of AlCl 3 in an ethanol-water solvent system, Bioresour. Technol. 116 (2012) 190–194, https://doi.org/10.1016/j.biortech.2012.03.126.
[52] W.N.P. van der Graaff, C.H.L. Tempelman, G. Li, B. Mezari, N. Kosinov, E.A. Pidko, E.J.M. Hensen, Competitive Adsorption of Substrate and Solvent in Sn-Beta Zeolite During Sugar Isomerization, ChemSusChem 9 (2016) 3145–3149, https://doi.org/10.1002/cssc.201600800.
[53] B.F.M. Kuster, The influence of water concentration on the dehydration of d-fructose, Carbohydr. Res. 54 (1977) 177–183, https://doi.org/10.1016/S0008-6215(00)84807-7.